International Biodeterioration & Biodegradation 177 (2023) 105531

Contents lists available at ScienceDirect

International Biodeterioration & Biodegradation

journal homepage: www.elsevier.com/locate/ibiod

Oxalate found in wood cell wall during incipient brown rot degradation

Sophie Füchtner [a], Gry Alfredsen [b], Lisbeth G. Thygesen [a,*]

[a] Department of Geosciences and Natural Resource Management, University of Copenhagen, Rolighedsvej 23, 1958, Frederiksberg, Denmark
[b] Department of Wood Technology, Norwegian Institute of Bioeconomy Research, P.O. Box 115, NO-1431, Ås, Norway

ARTICLE INFO

Keywords:
In situ localization
Picea abies
Raman microscopy
Rhodonia placenta

ABSTRACT

Brown rot fungi are a marvel and an enigma of Nature. They are capable of depolymerizing holocellulose within wood cell walls without significantly mineralizing lignin. The exact details behind this feat remain unknown, but a staggered mechanism has been identified: 1) an initial step characterized by oxidative degradation of the wood cell wall biopolymers and hypothesized to involve transport of Fe^{3+} chelated by oxalate into the cell wall, and 2) a second degradation step dominated by hydrolytic enzymes, primarily endoglucanase activity. We subjected spruce wood (*Picea abies*) to *Rhodonia placenta* and isolated xylem tissue in the initial stage of degradation. Confocal Raman microscopy revealed oxalate accumulation in the secondary cell wall of a tracheid having fungal hyphae within the lumen. This observation is the first *in situ* verification of oxalate accumulation within the cell wall during the first step of brown rot degradation.

1. Introduction

Brown rot fungi have been found to degrade wood in a staggered process where the first step is characterized by oxidative disruption of the cell wall, and the second by hydrolytic enzyme activity (Zhang et al., 2016). Since 1997 the first step has been hypothesized to involve transport of Fe^{3+} chelated by oxalate from the cell lumen and into the cell wall (Goodell et al., 1997). In the cell wall, Fe^{3+} is thought to be reduced to Fe^{2+} and take part in the Fenton reaction, during which short-lived hydroxyl radicals are generated that successively break covalent bonds in biopolymers at a safe distance from the hyphae (Arantes and Goodell, 2014). Already in 1991 *in situ* localization of fungal metabolites, either enzymatic or nonenzymatic, was found using immuno-electron microscopic localization (Kim et al., 1991). Specifically, brown rot fungi secrete oxalic acid and are capable of degrading oxalate, and oxalic acid/oxalate is assumed to have an iron transport function, contribute to pH regulation, and take part in the spatiotemporal regulation of the two degradative steps (Arantes and Goodell, 2014; Goodell et al., 1997). While low concentrations of oxalate at the hyphal front may promote Fenton chemistry, high concentrations behind the hyphal front may protect endoglucanases against radicals by immobilizing iron (Presley et al., 2018). For oxalate to have these functions, it must be present within the wood cell wall during active brown rot degradation, but *in situ* verification has so far not been presented. In the study described here, Raman microscopy combined with chemometrics was employed to study the cell wall of a tracheid where hyphae surrounded by Ca-oxalate crystals were present in the lumen.

2. Materials and methods

2.1. Sample preparation

Picea abies (L.) heartwood sticks with dimension 50 × 4 × 4 mm (longitudinal x radial x tangential) were cut from a wood disc as described in detail in Füchtner et al. (2020), which describes the experiment from which the current study emerged. The sticks were extracted with a series of four solvents under elevated pressure (1.38 MPa) using an Accelerated Solvent Extractor (DionexTM ASETM 350 Thermo Electron A/S, Scientific Instrument Division, 2650 Hvidovre, Denmark). The solvents were purchased from Sigma-Aldrich and consisted of heptane (99%, anhydrous), dichloromethane (≥99.8%, SupraSolv®), ethanol (96%, SupraSolv®) and demineralized water. Nine extraction cycles (5 min each) were used for each solvent at a temperature of 90 °C, except for ethanol where 100 °C were used. However, a fraction of the extractives remained within the sticks. Further details can be obtained in (Füchtner et al., 2020).

2.2. Fungal degradation

Nine extracted sticks were selected for degradation with *Rhodonia*

* Corresponding author.
E-mail address: lgt@ign.ku.dk (L.G. Thygesen).

https://doi.org/10.1016/j.ibiod.2022.105531
Received 14 July 2022; Received in revised form 11 November 2022; Accepted 14 November 2022
Available online 21 November 2022

placenta (Fr.) Niemelä, K.H. Larss. & Schigel (FPRL280, syn.: *Postia placenta*). Each stick was placed vertically on an already infected spruce feeder strip, and the fungus allowed to grow upwards in the longitudinal direction of the stick (adapted from (Zhang et al., 2016)) to obtain a degradation gradient from the bottom to the top of the stick capturing different phases of the fungal attack. The procedure is described in detail in (Füchtner et al., 2020). The fungus was allowed to grow to 2/3 of the sticks' height and harvested after 14 days. A small portion of the mycelium was carefully removed from one of the sticks, dried at 40 °C, and stored between glass slide and cover glass until Raman measurements. To minimize changes due to rapid drying, the frozen wood samples were placed in glass vials in a desiccator with dry silica under vacuum and placed in an oven at 60 °C for 24h (Füchtner et al., 2020). The stick with a weight loss closest to the mean was chosen for Raman imaging. The stick was sectioned into 15–20 μm sections at about 250 μm below the marked hyphal front using a Leica RM2255 microtome. In preparation for Raman imaging, sample sections were mounted on glass slides with water, covered with a cover glass, and sealed with nail polish.

2.3. Confocal Raman imaging

Imaging was performed on a WITec alpha 300R confocal Raman microscope (WITec GmbH, Lise-Meitner-Str. 6, D-89081 Ulm, Germany) using a 532 nm excitation laser. With the UHTS300 spectrometer (VIS), a spectral resolution of 3.8 cm^{-1} is achieved. An image of Norway spruce tracheids with opaque cell lumina was acquired with a laser power of 10 mW and 0.1 s integration time, using a 100x oil immersion objective (Zeiss EC "N-Achroplan", NA = 1.2, WD = 0.29 mm; Carl Zeiss GmbH; Jena, Germany). The resulting spatial resolution was 333 nm. Additionally, several single spectra of the opaque lumen content in cells distant from the imaged cells were acquired. Two images of R. placenta mycelium were recorded without the cover glass using a 100x air objective (Zeiss EC "Epiplan-Neofluar" DIC, NA = 0.9, WD = 0.31 mm, Carl Zeiss GmbH; Jena, Germany) at 69 mW laser power and 0.5 s integration time. Raman spectra of iron(II) oxalate dihydrate and Ca-oxalate hydrate (Sigma-Aldrich) were obtained using the same instrument as above, but equipped with a 10x air objective. Iron(II) oxalate spectra were captured as an average of 50 scans using 10 mW and Ca-oxalate hydrate spectra as an average of 10 scans using 60 mW. An integration time of 0.1 s was used in both cases. The spectra presented in this study were averaged over three locations.

2.4. Data analysis

Data were processed in MATLAB 2019a (The MathWorks, Inc., 1 Apple Hill Drive, Natick, MA 01760–2098).

2.5. Preprocessing

Spectra from wood and fungus were preprocessed in the same way. First cosmic rays were removed with a 3rd order median filter. The raw data of each image were split into groups using K-means cluster analysis (KMCA) and each group base line corrected separately using an asymmetric least squares algorithm adapted from (Eilers, 2004), adapting the two relevant parameters p and λ as needed (p = 0.0001–0.0003, λ = 1e5). The data were de-noised by principal component analysis (PCA) and reconstructed from 15 principal components. First derivatives were calculated from a 2nd order Savitzky-Golay filter (window size 11) and the spectral ranges of 250–1750 cm^{-1} and 2530-3740 cm^{-1} removed for data reduction.

2.6. Data analysis

An image of the mycelium of *R. placenta* was clustered with K means cluster analysis (5 repetitions) and the average spectrum extracted from the cluster with highest intensity. A rectangular area of the lumen was cut out and analyzed separately. The rest of the image was clustered with k means cluster analysis (5 repetitions). The cell with opaque lumen was cut out and only the clusters covering the S2 cell wall, as well as the lumen interface area were retained. Each of the resulting datasets (lumen and cell wall) were decomposed into constituting components and corresponding concentration profiles by multivariate curve resolution – alternating least squares (MCR-ALS) using the MCR-ALS GUI 2.0 (Jaumot et al., 2015) available for MATLAB. The spectra for initialization of the MCR-ALS algorithm were obtained based on the purest zero-order data selected by the SIMPLISMA algorithm (10% noise margin). The corresponding first-derivatives were used for MCR-ALS decomposition. The algorithm was constrained to not allow negative values in the concentration profiles (non-negativity constraint, Fast-Non-Negative-Least-Squares), but not in the component spectra, due to the use of first derivatives. The components were constrained by normalization with the Euclidean norm, in order to represent quantitative information in the concentration profiles. Finally, the zero-order spectra were reconstructed from the components (obtained as first derivatives) using the Penrose-Moore pseudoinverse (Barata and Hussein, 2012). The whole procedure is described in detail in (Füchtner et al., 2020). To verify the components obtained from decomposition of the cell lumen, the single spectra taken from other cells with opaque lumen spaces were analyzed together with the identified component spectra by PCA (first derivatives). For cross validation 25% of the data were left out using the venetian blinds methods (4 data splits, blind thickness 1). With 3 PCs 80.18% of the variance was explained (RMSEC 0.01653, and RMSECV 0.0257). The cell wall data were decomposed by MCR-ALS as above. A spot in the S2 clustered with the lignin-rich cell corners. Ten spectra located in the spot were averaged.

3. Results

Raman data of incipient brown rot degradation show presence of hyphae, cell wall degradation products and Ca-oxalate crystals in the tracheid lumen (Figs. 1 and 2) and of oxalate in the cell wall (Fig. 3). These results are presented below.

The lumen Raman data was deconvoluted using a five component MCR-ALS model, which had a lack of fit (LOF) of 3.94% and R^2 of 99.85% (Fig. 2). Based on comparison to average spectra obtained from mycelium of *R. placenta* (Fig. 1c) and of other brown rot fungi (De Gussem, 2007), one component was interpreted as signal from fungal mycelium. In a similar way, two model components were interpreted as signal from metal-oxalates, differing only by the relative intensities of the main bands, i.e., 1479 and 911 cm^{-1}. Band positions corresponded well with the Raman spectrum of Ca-oxalate dihydrate (Edwards et al., 2003) known to be predominantly produced by wood degrading fungi (Conolly et al., 1996). Additionally, the presence of oxalic acid was evident from the bands at 1740 and 478 cm^{-1} (Ma et al., 2013). Reference spectra of Ca-oxalate hydrate and Fe(II)-oxalate dihydrate are shown for comparison (Fig. 2c). These spectra show an additional band at 504 and 522 cm^{-1}, not reported in literature, but close to the 509 cm^{-1} band seen in the component spectra. Several single spectra of the lumina of other wood cells confirmed these findings (Fig. 2b,d). The remaining two components indicated low amounts of lignin and cellulose (Fig. 2d), but carbohydrate bands appeared reduced, as also observed in brown rot degraded Scots pine (Belt et al., 2019). A broad band was seen between 1350 and 1370 cm^{-1}. This might correspond to monomeric carbohydrates from cellulose and hemicelluloses (De Gelder et al., 2007).

Within the cell wall, a lignin-rich spot was seen in the middle of the S2 area (arrow in Fig. 3a), potentially a pit. The average spectrum of this region is shown in Fig. 3b. Evidence for the presence of oxalate in this location was directly observable via the band visible as a shoulder at 1479 cm^{-1} (Ca-oxalate dihydrate (Edwards et al., 2003), as well as the fingerprint band at 478 cm^{-1} (oxalic acid (Ma et al., 2013)). While weak, these absorbance bands correspond to those observed for oxalate in the

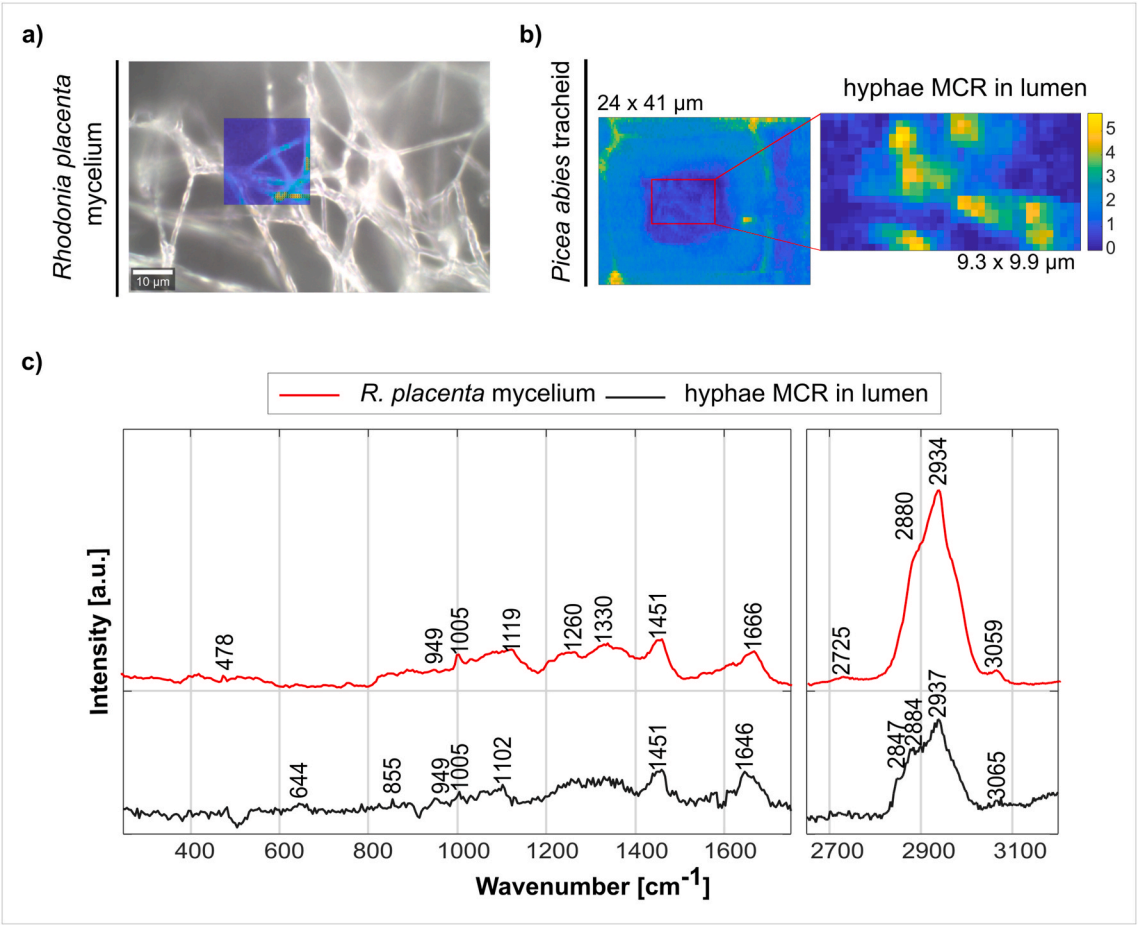

Fig. 1. Fungal hyphae and their Raman spectra. a) Light microscopy image of *R. placenta* mycelium overlaid with the acquired Raman image (color-coded intensity map showing the area under each spectrum). The most intense pixels were used to generate the reference spectrum shown in panel c. The respective pixels are maked with „x" in Fig. S1 of the supplementary information, b) Raman image of tracheid cell at the hyphal front investigated in this study with lumen area analyzed by MCR-ALS (red square). Enlargement shows the intensity map of the model component interpreted as fungal hyphae, c) Raman spectra of *R. placenta*: average spectrum of the mycelium (red) identified in the Raman image shown in panel a, and MCR-ALS component spectrum (black) from modelling of the lumen area denoted in panel b. The similarity between the two spectra in panel c strengthens the interpretation of the MCR-ALS component in panel b as fungal hyphae in the lumen.

lumen (Fig. 2d), and like the reference spectra in Fig. 2c, the average cell wall spectrum from this region had an additional so-far unreported band at 518 cm^{-1}.

MCR-ALS analysis of the spectra from the cell wall region (clusters 1 and 4 in Fig. 3a) resulted in a model with five components (LOF: 3.16%, R2: 99.90%, Fig. 3c and d). Three of these were interpreted as mixtures of cell wall polymers, with one having large contributions from lignin (C1) and two having large contributions from cellulose with two orientations (C2-3 (Gierlinger and Schwanninger, 2006)). In addition, the model evidenced the presence of oxalate distributed spot-wise in the S2 layer (C4), via bands at 1479, 906 and 482 cm^{-1}. These bands were stronger at the lumen-cell wall interface, resulting in a separate component (C5). Component C4 indicates that in locations with increased presence of oxalate, more changes in the cell wall polymers appeared to have occurred than elsewhere in the cell wall. Lignin de-methoxylation is suggested by the reduction of the band at 1455 cm^{-1} (C–H bending of methoxy groups (Bock and Gierlinger, 2019)), revealing bands at 1462 and 1479 cm^{-1}. These can both be attributed to cellulose (6), but due to the simultaneous presence of other oxalate bands at 482 and 906 cm^{-1}, we attribute the 1479 cm^{-1} signal to oxalate. Another interesting feature of the C4 component spectrum in Fig. 3d is the appearance of an intense band at 1630 cm^{-1}. The 1630 cm^{-1} band might be indicative of oxalate accumulation, as hydrated forms of both oxalic acid and various metal-oxalates show vibrations around this wavenumber ((Edwards et al., 2003; Ma et al., 2013) and Fig. 2c). Belt et al. (2019) also observed the appearance of this band after four weeks of fungal degradation and interpreted it as heartwood degradation products. The band position indicates either C═C or C═O stretches (Larkin, 2011). Carboxylic acids have been observed in cotton cellulose degraded by *R. placenta* or Fenton reagents (Arantes and Goodell, 2014). Side chain oxidations of lignin could also lead to the formation of carboxylic acids (Arantes and Goodell, 2014). Although Raman scattering of C═C stretches tends to be more intense than C═O stretches (Larkin, 2011), we find the formation of CC double bonds unlikely in an oxidative environment. However, as mentioned above, in the present case we are more inclined to attribute the 1630 cm^{-1} band to oxalate than to degradation products.

4. Discussion

It is well known that fungi may form crystals of Ca-oxalate surrounding their hyphae in the cell lumen (Conolly et al., 1996; Schilling, 2006), and this was also seen here. Likewise, oxalic acid has frequently been reported to be secreted in early fungal growth stages (Presley et al., 2018; Schilling, 2006). Previous *in situ* detection of components from the brown rot decay mechanism includes immunotransmission electron microscopy visualising unidentified high-affinity iron-binding compounds (Jellison et al., 1991) and cytochemical localization of H_2O_2 production during using transmission electron microscopy (Kim et al., 2002). What sets the present study apart from previous observations is

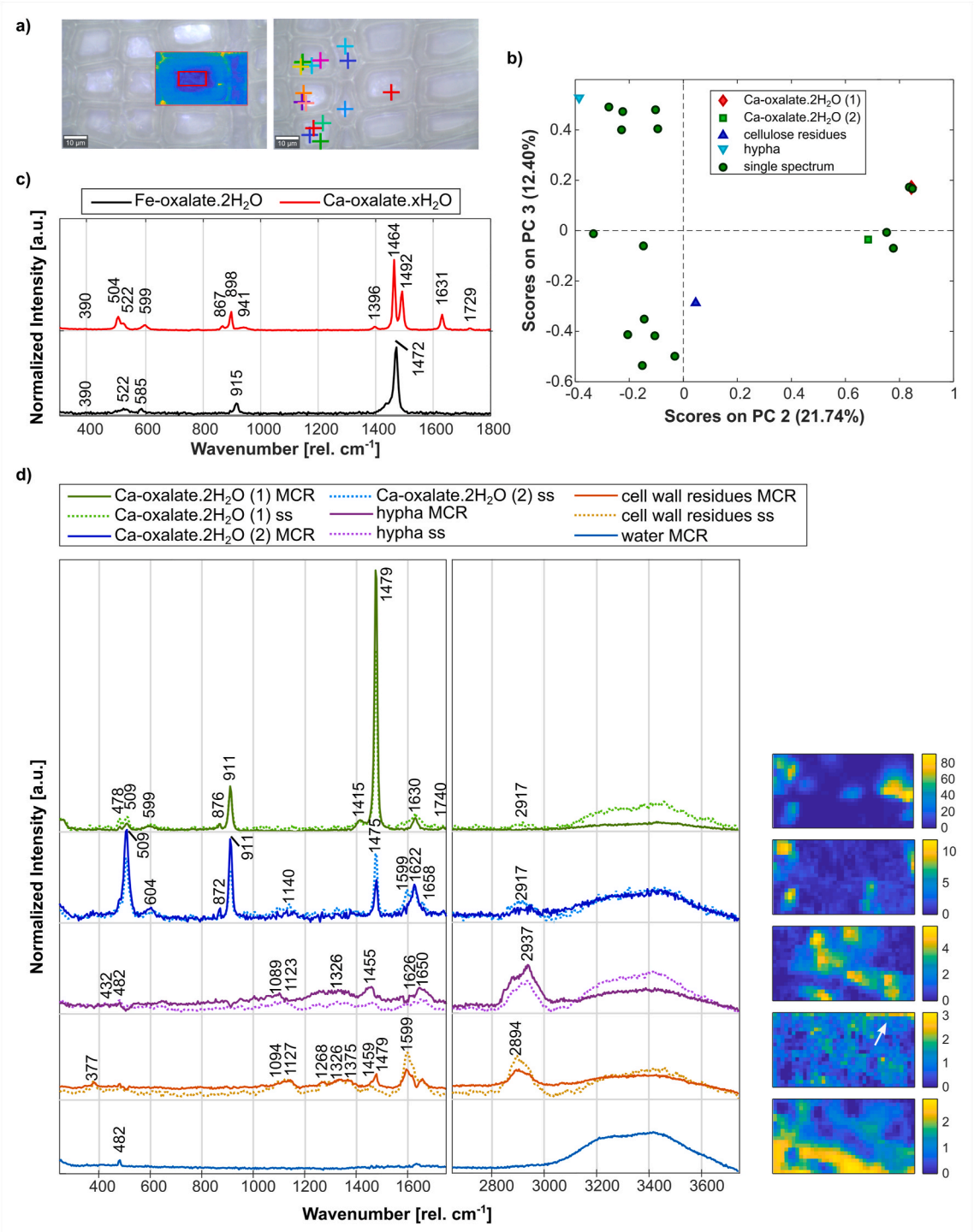

Fig. 2. Analysis of Raman data from the lumen of tracheids. a) Light microscopy images of *P. abies* sections showing the sampling locations of: left - the tracheid cell investigated in this study (shown by overlay with Raman image, which measures 24 × 41 μm) and showing the lumen area analyzed separately (red rectangle); right - single spectra of lumen content of various tracheid cells (ss, colored crosses). b) Scores plot from a PCA performed on the single spectra from panel a together with component spectra obtained by MCR-ALS of the lumen (panel d), and identified based on literature (7, 8). The scores plot shows grouping of the single spectra with identified component spectra, indicating that the lumen content of tracheids at distinct locations of the wood section are alike. c) Reference spectra of Ca-oxalate monohydrate and Fe(II)-oxalate dihydrate, d) MCR-ALS component spectra (MCR) of the lumen of the imaged tracheid cell overlaid with the corresponding averaged single spectra (ss) as indicated by PCA in panel b and showing great similarity. On the right, the distribution maps of the corresponding components of the lumen model. Oxalate was found in the form of two crystal polymorphs of Ca-oxalate in close proximity to fungal hyphae. Furthermore, cell wall residues and water from sample preparation were detected.

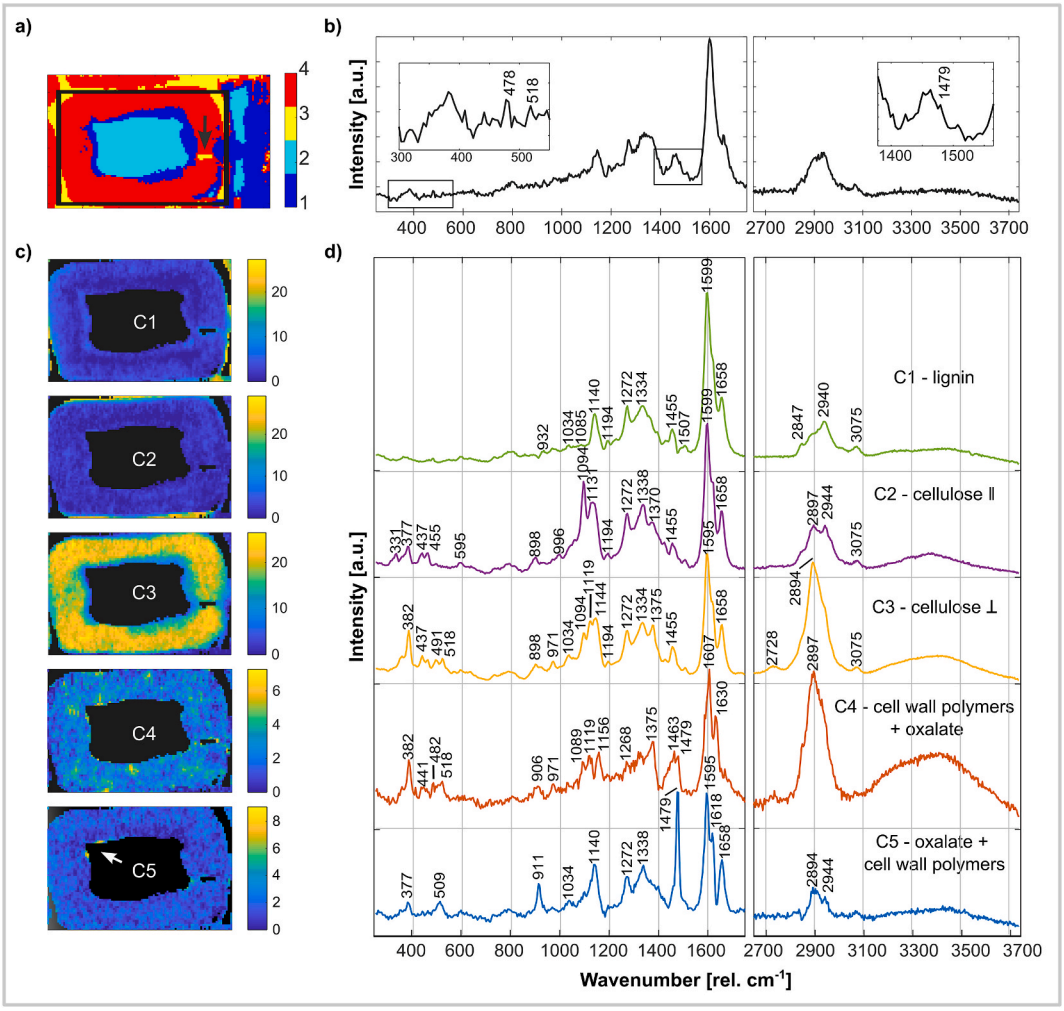

Fig. 3. Analysis of Raman data of the cell wall of a tracheid using cluster analysis (a and b) and MCR-ALS (c–d). a) Result of K-means cluster analysis of the image. The black frame shows the area from which the cell wall spectra (S3 and S2 layers, respectively clusters 1 and 4) were extracted, b) average spectrum extracted from a spot of cluster 3 located in the S2 cell wall area (black arrow in panel a) and showing signs of oxalate. c) Distribution maps of the MCR-ALS components shown in d) as obtained from the cell wall model. Image size: 24 × 41 μm.

the *in situ* verification of oxalate accumulation in the cell wall (Fig. 3). Even though the exact details explaining the reduction of Fe^{3+} to Fe^{2+} during the initial oxidative brown rot biopolymer depolymerization is still under debate, it is generally agreed that fungal secretion of oxalic acid plays an important role in the process by solubilizing iron and regulating pH to make sure the reduction of Fe^{3+} can only take place at a distance from the hypha (Arantes and Goodell, 2014; Presley et al., 2018; Schilling, 2006; Zhu et al., 2022). That oxalate takes part in transport of Fe^{3+} into the cell wall has been assumed.

5. Conclusion

Our finding provides direct evidence of oxalate accumulation in the cell wall during the oxidative stage of initial brown rot degradation and strengthens the hypothesis of the important role of oxalate in the brown rot degradation mechanism.

Declaration of competing interest

The authors declare that they have no known competing financial interests or personal relationships that could have appeared to influence the work reported in this paper.

Data availability

Data will be made available on request.

Acknowledgments

SF and LGT thank Klaus Richter and Annika Pilgaard at the Technical University of Munich for collaboration on brown rot degradation. Funding: LGT and GA thank VILLUM Fonden (project no. 12404) respectively the Research Council of Norway (project no. 302072) for funding.

Appendix A. Supplementary data

Supplementary data to this article can be found online at https://doi.org/10.1016/j.ibiod.2022.105531.

References

Arantes, V., Goodell, B., 2014. Current Understanding of Brown Rot Fungal Biodegradation Mechanisms: A Review. Deterioration and Protection of Sustainable Biomaterials. American Chemical Society. https://doi.org/10.1021/bk-2014-1158.ch001.

Barata, J.C.A., Hussein, M.S., 2012. The moore-penrose pseudoinverse: a tutorial review of the theory. Braz. J. Phys. 42, 146–165. https://doi.org/10.1007/s13538-011-0052-z.

Belt, T., Altegen, M., Makela, M., Hanninen, T., Rautkari, L., 2019. Cellular level chemical changes in Scots pine heartwood during incipient brown rot decay. Sci. Rep. 9 https://doi.org/10.1038/s41598-019-41735-8.

Bock, P., Gierlinger, N., 2019. Infrared and Raman spectra of lignin substructures: coniferyl alcohol, abietin, and coniferyl aldehyde. J. Raman Spectrosc. 50, 778–792. https://doi.org/10.1002/jrs.5588.

Conolly, J.H., Arnott, H.J., Jellison, J., 1996. Patterns of calcium oxalate crystal production by three species of wood decay fungi. Scanning Microsc. 10, 385–400.

De Gelder, J., De Gusem, K., Vandenabeele, P., Moens, L., 2007. Reference database of Raman spectra of biological molecules. J. Raman Spectrosc. 38, 1133–1147. https://doi.org/10.1002/jrs.1734.

De Gussem, K., 2007. Optimisation of Raman Spectroscopy for the Analysis of Basidiomycota: Spores, Latex and Mycelium. PhD Thesis. Ghent University, Gent, Belgum. https://doi.org/10.13140/RG.2.1.1646.4484.

Edwards, H.G.M., Seaward, M.R.D., Attwood, S.J., Little, S.J., De Oliveira, L.F., Tretiach, M., 2003. FT-Raman spectroscopy of lichens on dolomitic rocks: an assessment of metal oxalate formation. Analyst 128, 1218–1221. https://doi.org/10.1039/b306991p.

Eilers, P.H.C., 2004. Parametric time warping. Anal. Chem. 76, 404–411. https://doi.org/10.1021/ac034800e.

Füchtner, S., Brock-Nannestad, T., Smeds, A., Fredriksson, M., Pilgård, A., Thygesen, L. G., 2020. Hydrophobic and hydrophilic extractives in Norway spruce and kurile larch and their role in Brown-rot degradation. Front. Plant Sci. 11 https://doi.org/10.3389/fpls.2020.00855.

Gierlinger, N., Schwanninger, M., 2006. Chemical imaging of poplar wood cell walls by confocal Raman microscopy. Plant Physiol. 140, 1246–1254. https://doi.org/10.1104/pp.105.066993.

Goodell, B., Jellison, J., Liu, J., Daniel, G., Paszczynski, A., Fekete, F., Krishnamurthy, S., Jun, L., Xu, G., 1997. Low molecular weight chelators and phenolic compounds isolated from wood decay fungi and their role in the fungal biodegradation of wood. J. Biotechnol. 53, 133–162. https://doi.org/10.1016/S0168-1656(97)01681-7.

Jaumot, J., de Juan, A., Tauler, R., 2015. MCR-ALS GUI 2.0: new features and applications. Chemometr. Intell. Lab. Syst. 140, 1–12. https://doi.org/10.1016/j.chemolab.2014.10.003.

Jellison, J., Chandhoke, V., Goodell, B., Fekete, F.A., 1991. The isolation and immunolocalization of iron-binding compounds produced by *Gloeophyllum trabeum*. Appl. Microbiol. Biotechnol. 35, 805–809. https://doi.org/10.1007/BF00169899.

Kim, Y.S., Goodell, B., Jellison, J., 1991. Immuno-electron microscopic localization of extracellular metabolites in spruce wood decayed by Brown-rot fungus. Postia placenta 45 (5), 389–393. https://doi.org/10.1515/hfsg.1991.45.5.389.

Kim, Y.S., Wi, S.G., Lee, K.H., Singh, A.P., 2002. Cytochemical localization of hydrogen peroxide production during wood decay by Brown-rot fungi. *Tyromyces palustris* and *Coniophora puteana* 56 (1), 7–12. https://doi.org/10.1515/HF.2002.002.

Larkin, P., 2011. IR and Raman Spectroscopy: Principles and Spectral Interpretation. Elsevier Inc. https://doi.org/10.1016/B978-0-12-386984-5.10001-1.

Ma, Q.X., He, H., Liu, C., 2013. Hygroscopic properties of oxalic acid and atmospherically relevant oxalates. Atmos. Environ. 69, 281–288. https://doi.org/10.1016/j.atmosenv.2012.12.011.

Presley, G.N., Zhang, J.W., Schilling, J.S., 2018. A genomics-informed study of oxalate and cellulase regulation by brown rot wood-degrading fungi. Fungal Genet. Biol. 112, 64–70. https://doi.org/10.1016/j.fgb.2016.08.004.

Schilling, J.S., 2006. Oxalate Production and Cation Translocation during Wood Biodegradation by Fungi. PhD, University of Maine.

Zhang, J.W., Presley, G.N., Hammel, K.E., Ryu, J.S., Menke, J.R., Figueroa, M., Hu, D.H., Orr, G., Schilling, J.S., 2016. Localizing gene regulation reveals a staggered wood decay mechanism for the brown rot fungus *Postia placenta*. Proc. Natl. Acad. Sci. U.S. A. 113, 10968–10973. https://doi.org/10.1073/pnas.1608454113.

Zhu, Y., Li, W., Meng, G.D., Li, X., Goodell, B., 2022. Non-enzymatic modification of the crystalline structure and chemistry of Masson pine in brown rot decay. Carbohydr. Polym. 286 https://doi.org/10.1016/j.carbpol.2022.119242.